Simulating Cervical Vertebrae Motion Using Elementary Contact Pairs

Andrés Kecskeméthy, Christian Lange and Gerald Grabner
Institute of Mechanics and Mechanisms, Technical University of Graz
Email: {kecskemethy | lange | grabner}@mechanik.tu-graz.ac.at

Dedicated to Professor Manfred Hiller on occasion of his 60th birthday.

Abstract

This paper describes some actual results from an ongoing project aimed at reproducing human cervical intervertebral motion using parallel manipulators. Described in the paper is the mathematical modelling of a vertebrae pair using multibody methods and impact analysis techniques with elementary contact geometry for the facet joints. The results are compared with existing approaches and with experimental data, showing a good agreement with the latter and an efficiency boost compared to existing approaches by a factor of 350. The investigations are focused on the vertebrae pair C5-C6 but can be easily extended to other vertebrae.

1 Introduction

In the reduction of medical costs, the improvement of human disease therapies, the development of new techniques for injury prevention measures, and many other fields related to human life, biomechanics is playing an increasingly important role. Hereby, the human spine is given particular attention, due to its frequent involvement in accident-induced injuries [1] and almost epidemic appearance in common diseases such as low back pain [26]. Areas of actual intense research in this setting are, among others, the development and surgical placement of spinal prosthetic devices such as spine implants, effective spinal immobilizers and spine braces [7], design of reliable anthropomorphic test devices (ATD) for physical crash-worthiness simulations [31], and the *in vivo* and *in vitro* estimation of biological spine parameters [2, 16]. In this setting, reconstruction of inter-vertebral motion, although basically understood, still poses many open problems. This is so because pairs of vertebrae undergo in general six-dimensional motion relative to one another, but display a high degree of coupling between gross translational and rotational degrees-of-freedom due to restraints imposed by ligaments and muscles and the compliant nature of the inter-vertebral discs [30]. These degrees of freedom are excited differently depending on loading conditions and biological parameters, making it difficult to establish relevant kinematic parameters on a case-by-case basis, as required, e.g., to identify spinal diseases or to mimic the effects of a surgical therapy for a concrete person. Hence, predictions often fail to match experimental measurements, as is the case in particular in vehicle crash situations [9].

Models in biomechanics can be roughly divided in four categories: (a) physical models, (b) *in vitro* models, (c) *in vivo* models, and (d) computer models (see Table 1). All of these models are sometimes also called surrogate mechanisms, although mostly one understands as a surrogate a physical model. In the setting of this article, we are interested mainly in a computer model, although the final aim of the project is to develop a physical mechanism for vertebrae pair motion simulation.

	uses	advantages	disadvantages
physical model	implant and component testing	simple, less variable, less expensive, evaluates implant alone	non-anatomic, un-physiologic implant loading
In vitro model			
animal	implant testing	cheaper, less variable	different anatomy and biomechanics, and does not represent human variability
human	spinal function and dysfunction studies, and implant testing	actual human anatomy, physical properties, and population variability	difficult to obtain, expensive, more variable than animal
In vivo model			
animal	studying phenomena that occur *in vivo*, e.g., fusion and adaptation	essential for studying fusion, adaptation, and effects of drugs	different anatomy, biomechanics, and biology, and has greater variability than *in vitro* animal model
human	studying living phenomena in humans, e.g., muscle recruitment	actual human responses to external stimulus, e.g., head kinematics and muscle recruitment in whiplash simulations	subjects cannot be loaded to cause any injury
mathematical model	simulating situations not modeled by other biomechanical models	capable of simulating real phenomena-effects of muscles, bone healing, tissue adaptation, determining internal loads, strains and stresses	difficult to validate, tendency to use the model beyond its validation boundaries

Table 1: Categories of biomechanical models (from [22]).

Existing approaches for computer modelling of inter-vertebral motion use either kinematic or full-scale finite element (FEM) models to reproduce vertebrae interaction. Kinematic methods regard mainly planar flexion and extension motion in the sagittal plane, employing the notion of instantaneous axes of rotation (IAR) to reproduce combined rotation and translation between pairs of vertebrae [30]. These axes act as virtual hinges connecting pairs of vertebrae, where the virtual pivot point is located somewhere between the centers of the two connected vertebrae and the center of the inter-vertebral disc [12]. They embody the well-known first-order approximation of planar motion in kinematics [3]. The problem with this approach is that the location of the IAR varies with respect to flexural position as well as with respect to clinical and personal data (age, sex) of the target person. Moreover, the IAR approach is not easily extendible to full-degree-of-freedom joints, such as occurs in a combined flexion-extension and lateral or axial rotation of the spine. On the other hand, FEM modelling allows one to take into consideration full effects of the mechanics of inter-vertebral motion, including contact mechanics, surface gliding, and deformation. For such models, a number of now industry-standard programs have been developed, such as MADYMO [15], ATB [20], and LS-DYNA3D [1]. However, these models have the drawback that for actual computations, a great number of biological parameters are required that are difficult to impossible to obtain. Moreover, the computer models are computationally very slow, prohibiting their use for real-time simulations, as required for educational or optimization purposes. This also hampers their immediate use in medical applications, where fast, online rendering of motion properties is necessary to assess the effects of therapeutic measures.

Based on finite-element and multibody methods, and their combination, an enormous improvement of motion-simulation capabilities for the human spine has been achieved in the last three decades. A three-dimensional mathematical model of the human spine structure using rigid bodies, springs, and dashpots is presented in Panjabi (1973) [21]. The model comprises up to 21 stiffness and damping coefficients per vertebrae pair, but no contact and lift-off effects. Huston and Advani (1979) describe a comprehensive three dimensional model of the human head and neck [11]. This model predicts the displacements, velocities, and accelerations of the center of mass of the head and neck resulting from contact and/or inertial impact forces. The model, incorporating key anatomical components and joint limits, was validated by comparison with direct frontal and occipital impact experiments on human cadavers, and sled tests conducted on human volunteers. Goldsmith et al. (1984) [10] performed computations for side blows and compared them with corresponding data obtained from either a physical model replicating a human head-neck system or from volunteer response to side acceleration. Deng [6] developed a comprehensive mechanically equivalent human head-neck-upper-torso system comprising kinematics, muscle stresses and strains, disc pressures, intracranial pressures and skull strains. Moreover, a three-dimensional numerical model for predicting the human body response under dynamic loading is given and compared with the physical results from other investigations.

Mathematical head-neck models for acceleration impacts are described further by de Jager [5]. First, he introduces a relatively simple model with few anatomic details, the so called *global head-neck model*, comprising a rigid head and rigid vertebrae, connected through three-dimensional nonlinear viscoelastic elements for the intervertebral joints. These joints describe the lumped mechanical behavior of the intervertebral disc, ligaments and facet joints. The model was calibrated to match the response of human volunteers to frontal impacts. Furthermore, *detailed segment models* of the upper and lower cervical spine were developed as an intermediate step. These models comprise rigid bodies for the vertebrae, three-dimensional linear viscoelastic elements for the intervertebral disc, nonlinear viscoelastic line elements for the ligaments, and frictionless contact interactions between the the facet joints. Finally, a *detailed head-neck model* was formed by joining the *detailed segment models* and adding muscle elements. This model comprises a rigid head and rigid vertebrae, linear viscoelastic discs, frictionless facet joints, nonlinear viscoelastic ligaments and contractile Hill-type muscles.

Intensive studies of the geometry of the vertebrae are reported in Nissan et al. [19] using X-rays of the cervical and lumbar region in normal, healthy men. Panjabi et al. [23] determined the three-dimensional quantitative anatomy of the middle and lower cervical vertebrae by measuring the three-dimensional coordinates of various marked points on the surface of the vertebra with a specially designed morphometer instrument. From theses coordinates, linear dimensions, angulations, and areas of surfaces and cross-sections of most vertebral components were calculated. The influence of geometrical factors on the behavior of lumbar spine segments was reported by Robin [27]. He found that the geometrical factors do exert a noticeable influence on the behavior of the spine, especially those which interfere with the dimensions of the intervertebral disc.

The key issue in deriving biofidelic computer models lies in the determination of the biological parameters. An extensive study of the mechanical properties of the human spine cord can be found in [2]. Chazal et al. [4] report the results of a biomechanical study of 43 human spinal ligaments from fresh cadavers and living subjects. Myklebust et al. [18] perform experimental tests with spinal ligaments from 41 fresh human male cadavers *in situ* by sectioning all elements except the one under study and derive force-deflection curves with a sigmoidal shape and the force of failure. Pintar et al. [25] investigate tensile properties of the human intervertebral disc in tension. The influence of muscle morphometry and moment arms on the moment-generating capacity of human neck muscles was analyzed by Vasavada et al. [29] and the

morphometry of human neck muscles themselves by Kamibayashi et al. [13]. They found that the neck musculature was architecturally complex and that many muscles cross two or more joints and have multiple attachments to different bones. Moreover, the cross-sectional areas of neck muscles do not scale proportionally with body height and weight, nor do individual muscles with widely varying cross-sectional areas scale from one subject to another. For validation of computer models, Panjabi et al. [24] report static load-displacement curves as well as the neutral zones for six types of pure force loading of cervical spine specimens from fresh human cadavers. The load-displacement response and strength of the mid and lower cervical regions were determined for combinations of sagittal loads, *in vitro*, by Shea et al. [28] to provide basic informations for the *in vitro* investigation of passive cervical spine protection.

This paper deals with the mechanical modelling of the motion only between one pair of vertebrae of the human cervical spine, namely C5-C6. However, the underlying theory is developed in such a general way that other vertebrae pairs can be rapidly modeled correspondingly, when needed.

2 Basic Model Parameters

The motion of the cervical spine comprises flexion and extension (Fig. 1), lateral bending (Fig. 2) and axial rotation. Hence, in order to obtain full spine mobility, the model for the vertebrae pair must allow for relative six-degree-of-freedom motion, even in the presence of kinematical constraints, as specified below.

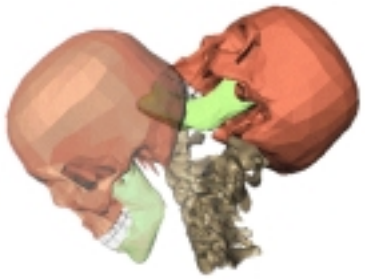

Figure 1: Flexion and extension.

Figure 2: Lateral bending.

As only relative motion interests in this setting, the lower vertebra C6 is fixed to the inertia system, to which the upper vertebra C5 is connected via a six-degree-of-freedom joint with three translations along the coordinate axes and three (consecutive) rotations about the same axes. In addition to the six-degree-of-freedom joint, motion constraints are introduced by (unilateral) contact elements reproducing the surfaces of the facet joints (Fig. 5). Moreover, the junction between the vertebrae is enforced by force-displacement elements comprising the intervertebral disc (Fig. 4) and the ligaments (Fig. 7), as explained below.

2.1 Structure and Inertia Properties

The definition of the reference coordinate systems is depicted in Fig. 3. The x-axis points to the front and the z-axis upwards. Table 2 summarizes the initial translations, s_x, s_z, of the origin of the upper body in x- and z-direction, respectively, and the relative rotation φ_y about the y-axis with respect to the lower body. The table also displays the inertia properties of the vertebrae.

name	mass	tensor of inertia			origin		center of gravity		orientation
	m	I_{xx}	I_{yy}	I_{zz}	s_x	s_z	g_x	g_z	φ_y
	kg	kg · cm^2			mm		mm		deg
C5	0.23	2.3	2.3	4.5	-2.8	17.4	-8.1	0.0	-5.2
C6	0.24	2.4	2.4	4.7	-2.0	18.4	-8.3	0.0	-5.6

Table 2: Inertia properties [5].

2.2 Intervertebral Disc

The intervertebral disc (Fig. 4) can be modeled by an anisotropic set of parallelly connected linear spring-damper elements. These elements incorporate also the effects of the uncovertebral joints. The elastic properties of the disc are computed according to Eq. (1), with F_i being the deformation and deformation-rate dependend force vector and M_i the twist and twist-rate dependend torque vector, respectively:

$$\begin{aligned} F_i &= k_{ti} \cdot t_i + b_{ti} \cdot v_i \\ M_i &= k_{\varphi i} \cdot \varphi_i + b_{\varphi i} \cdot \omega_i, \quad i = x, y, z \quad . \end{aligned} \tag{1}$$

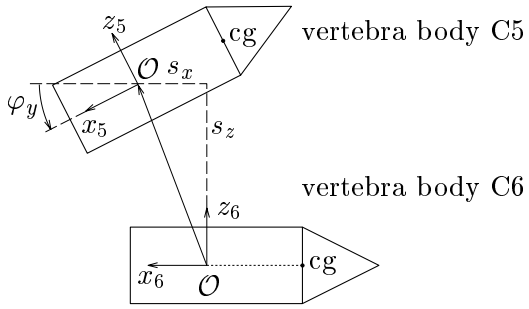

Figure 3: Definition of the reference systems [5].

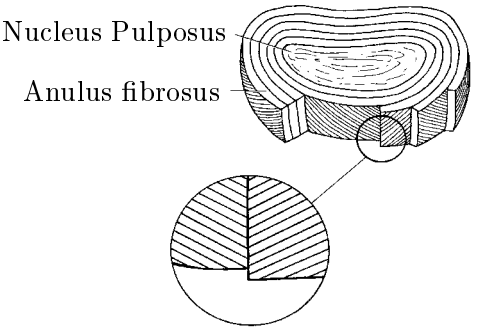

Figure 4: Intervertebral disc [8].

The numerical values for the stiffness coefficients k_{ti} and $k_{\varphi i}$ are taken from [17] and are summarized in Table 3. The load directions correspond to the six degrees of freedom of the relative motion of the vertebrae pair, namely anterior shear (AS) and posterior shear (PS) for x translation, lateral shear (LS) for y translation, tension (TNS) and compression (CMP) for z translation, lateral bending (LB) for x rotation, flexion (FLX) and extension (EXT) for y rotation, and axial rotation (AR) for z rotation. The damping coefficients for translation and rotation were taken as $b_{ti} = 1000$ Ns/m and $b_{\varphi i} = 1.5$ Nms/rad according to [5].

2.3 Facet Joints

In addition to the intervertebral disc, the vertebrae pair is partially guided by the facet joints, as shown in Fig. 5. These joints support only pressure contact forces and hence act as unilateral constraints comprising contact and free-flight phases. During contact, the roughly planar surfaces of the contact pair glide on each other with almost no friction. When the contact force

direction	AS	PS	LS	TNS	CMP	LB	FLX	EXT	AR
of load	N/mm					Nm/deg			
stiffness	62	50	73	68[a]	492	0.33	0.21	0.32	0.42

[a] taken from [25]

Table 3: Stiffness properties of intervertebral disc [17].

vanishes, the surfaces detach from each other, eliminating the geometric constraints induced by the facet joint temporarily. During this motion, the facet joints are pulled together by the sur-

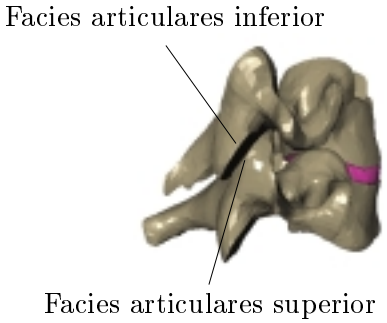

Figure 5: Facet joints.

rounding ligaments, which act as force elements. The surface of the facet joints can be modeled either as a perfectly planar cross section of a cylinder, or by hyper-ellipsoids

$$\left(\frac{|x|}{a}\right)^n + \left(\frac{|y|}{b}\right)^n + \left(\frac{|z|}{c}\right)^n = 1,\ n \geq 2\,, \tag{2}$$

where a, b, c are the semi-axes of the ellipsoid along the x, y and z- axes of the body fixed coordinate frame, respectively. For the position and orientation of the right facet one has to change the sign of the y-coordinate and the angle φ_x. Table 4 reproduces the geometric properties of an hyper-ellipsoid model employed in this work, where the order of the hyper-ellipsoid is taken as $n = 4$.

position of facet on left side	coordinates of center point			lengths of semi-axes			relative orientation	
	x	y	z	a	b	c	φ_y	φ_x
	mm			mm			deg	
C5 inferior	-13.7	20.3	-6.5	5.6	5.9	1.0	-45.6	13.8
C6 superior	-14.4	20.0	8.5	5.5	6.2	1.0	-50.8	-13.8

Table 4: Geometry data of facet joints [5].

In order to be able to reproduce the synovial behavior of the facet joints, the latter were modeled as frictionless compliant contact elements allowing for normal compression and producing contact forces linearly dependent on normal penetration and its time derivative. The normal contact

force F_c hence is determined by

$$F_c = b_f \cdot \dot{u} + \begin{cases} 2 \cdot 10^9 \cdot u^2 & \text{for} \quad 0 \le u \le 3 \cdot 10^{-4} \\ 180 + 1.2 \cdot 10^6 \cdot (u - 3 \cdot 10^{-4}) & \text{for} \quad u > 3 \cdot 10^{-4} \end{cases} , \tag{3}$$

where u represents the penetration, in meters, and $\dot{u}$ is the penetration rate, as measured in m/s. The damping coefficient b_f is set to $b_f = 300$ Ns/m according to [5].

2.4 Nonlinear Viscoelastic Ligaments

Six ligaments of the lower cervical spine are incorporated in the model, namely, the anterior longitudinal ligament (ALL), the posterior longitudinal ligament (PLL), the flaval ligament (FL), the interspinous ligament (ISL) and the left and right capsular ligament (CL), see Fig. 7.

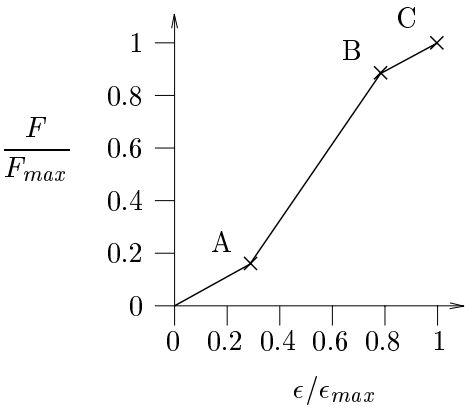

Figure 6: Dimensionless force-strain curve.

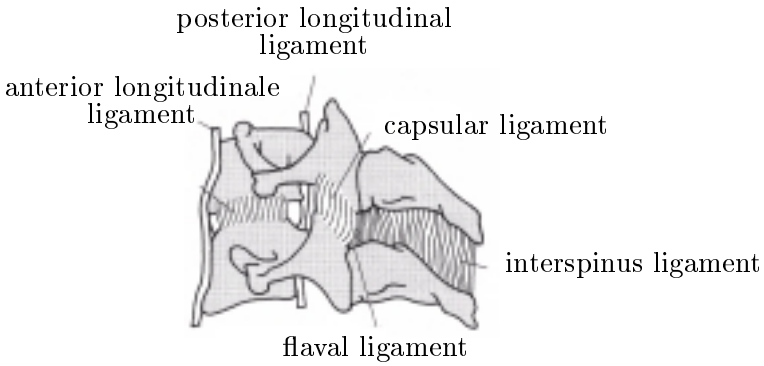

Figure 7: Ligaments [8].

The ligaments are modeled as *robes* transmitting only tension forces. These tension forces are functions of ligament elongation ϵ and its time derivative, namely

$$F_l = \begin{cases} F_{el}(\epsilon) + b_l \cdot \mathrm{d}\epsilon/\mathrm{d}t & \text{for} \quad \epsilon \ge 0 \\ 0 & \text{for} \quad \epsilon < 0 \end{cases} , \tag{4}$$

where the load-displacement curves $F_{el}(\epsilon)$ are taken as piecewise linear functions comprising three segments, as shown in Fig. 6. The corresponding numerical values of the support points A, B, C taken in this report are reproduced in Table 5, while the damping coefficient b_l was set to 300 Ns/m, corresponding to given patterns in the literature. The lengths of the ligaments in the undeflected case, l_0, can be found in Table 6 together with the corresponding assumed insertion points of the ligaments in body-fixed coordinates of the coordinate frame of the corresponding vertebra body.

3 MADYMO Model

MADYMO is the world-wide standard for occupant safety analysis. It is used extensively in industrial engineering, design offices, research laboratories and technical universities. It has proven itself in numerous applications, often supported by verification studies using experimental

ligament	A		B		C	
	ϵ/ϵ_{max}	F/F_{max}	ϵ/ϵ_{max}	F/F_{max}	ϵ_{max}	F_{max}/N
ALL	0.24	0.11	0.80	0.88	0.58	111
PLL	0.22	0.12	0.78	0.90	0.45	83
FL	0.33	0.21	0.77	0.89	0.21	115
ISL	0.33	0.19	0.78	0.87	0.40	34
CL (average)	0.28	0.16	0.78	0.88	0.42	108

Table 5: Elastic characteristic of the ligaments [5] (see also Fig. 6).

ligament	origin C5			origin C6			rest length
	x	y	z	x	y	z	l_0
ALL	7.7	0.0	0.0	8.0	0.0	0.0	18
PLL	-8.1	0.0	0.0	-8.3	0.0	0.0	17
FL	-25.4	0.0	-1.7	-26.3	0.0	-1.9	15
ISL	-39.9	0.0	-3.2	-47.3	0.0	-4.1	16
CL	-15.1	$\pm$20.3	-5.1	-12.9	$\pm$20.0	7.2	6

Table 6: Parameter of modeled ligaments in mm for spinal level C5–C6 [5].

test data[1]. For this reason, this package was chosen as the software platform for creating a reference computer model of the kinematic, static and dynamic intervertebral interactions. However, as it turns out, the algorithms employed in MADYMO render rather slow computer simulations, which prohibit the use of MADYMO models in real-time simulation, as needed for the realization of a control loop in the targeted surrogate mechanism. Hence, in parallel to the MADYMO model, customized models for intervertebral motion had to be developed, which shall be described in the next subsection.

One of the key properties of MADYMO is its input-output processing mode. To simulate a mechanical system, one hence has to write a data file according to certain rather strict syntax rules. Elements and parameters are specified by keywords and numerical data. The complete data file is then compiled and linked to the main MADYMO program, where the specified time interval is simulated. Results are written to several output files, depending on the user's specification. Interactions of the user during the simulation are not possible. After computation, the simulation can be visualized as a movie using the MADYMO post-processor.

An example how to specify a spring-damper element using the MADYMO keyword `Kelvin Element` is given below:

```
FORCE MODELS
KELVIN ELEMENT ALL
  SYSTEM  1
  BODY  1
  POINT  8.0e-3  0.0  0.0
  SYSTEM  2
  BODY  2
  POINT  7.7e-3  0.0  0.0
  L0   18.0e-3
```

[1] http://www.madymo.com

```
  LOADING FUNCTION  1
  UNLOADING FUNCTION  1
  HYS MOD  NONE
  DAMPING COEFFICIENT 300.00
END KELVIN
FUNCTIONS
! spring characteristic  epsilon(dl/l_0) vc. F
! ALL ------- LOADING FUNCTION:  1 --------------
  5
  -1.0       0.00
   0.0       0.00
   0.1392   12.21
   0.464    97.68
   0.58    111.00
  END FUNCTIONS
END FORCE MODELS
```

With the data set given in Section **2**, the motion of the vertebrae pair could be readily implemented in MADYMO. The facet joints were implemented as `Ellipsoid-Ellipsoid Contact Interactions` comprising hyper-ellipsoids of degree $n = 4$. For visualization purposes, vertebrae bodies were modeled as hyper-ellipsoids of degree $n = 2$, with no contact interactions arising from this model. Similarly, the vertebra arches are visualized as elongated hyper-ellipsoids of degree $n = 2$, which only have graphical meaning and do not provide any physical interactions with the environment. Moreover, in order to reduce computational overhead, only the hyper-ellipsoids embodying the facet joints are graphically rendered, without reproduction of the interconnection to the vertebra bodies. This crude graphical model suffices to verify motion results, while at the same time yielding acceptable simulation times for the computer runs (approx. 5.7 seconds per run).

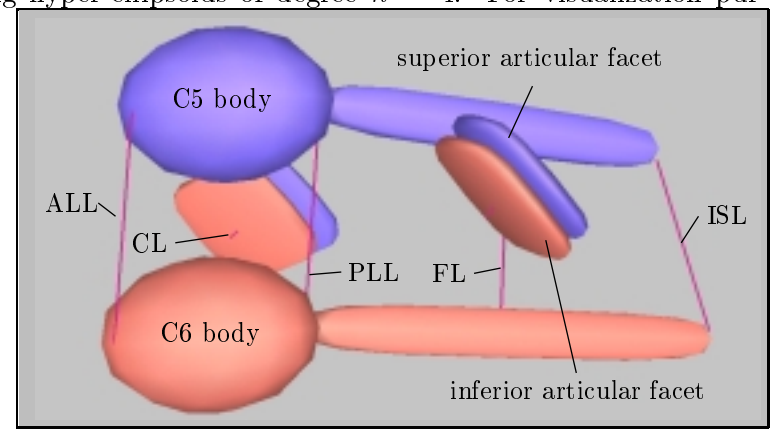

Figure 8: C5–C6 MADYMO ellipsoid model

To take care of the visco-elastic behavior of the intervertebral disc, the origins of the vertebra body reference systems were constrained by `Point-Restraints` for the translational part and by `Cardan Restraints` for the rotational part. The six included ligaments are specified as the above mentioned `Kelvin Elements`.

4 MOBILE Model

MOBILE is an object-oriented programming environment designed for the modelling of multibody systems [14]. One of its main features is the intuitive representation of mechanical entities as objects capable of transmitting motion and force across the system. Other features of MOBILE are the direct modelling of mechanical systems as executable programs or as modules for existing libraries. This yields an open building-block system design that allows the programmer to extend the provided library in any direction, in contrast to input-oriented pro-

gramming packages, where the user has to resort to built-in functions without the possibility of extending or adapting the employed algorithms. MOBILE is implemented in the object-oriented programming language C++, which assures portability and offers comfortable interfaces to three-dimensional graphic libraries for animation, such as *OpenInventor*. This makes direct user feedback and interaction possible, including click-and-drag features for online kinematics, statics and dynamics.

The objects of MOBILE are organized in three categories, namely, (a) basic mathematical objects, which provide the algebraic resources for performing the typical multibody calculations, (b) kinetostatic-state objects, which are used to store and retrieve kinematic or load-related information at specific locations of the multibody system, and (c) kinetostatic transmission elements, which transmit the information stored with the kinetostatic state objects from one location of the system to the other. Each transmission element supplies, according to its real-world counterpart, two basic operations: (I) transmission of motion and (II) transmission of forces.

For unilateral constraints, MOBILE supports the concept of state events, which fire when a given condition supplied by the user, such as beginning of penetration or vanishing of normal force, is fulfilled. With this feature, it is possible to compute quite accurately the effects of impacts, as is needed in the present setting for the modelling of facet joints.

4.1 Serial Model

The basic scaffolding of the relative kinematics and the statics of the vertebrae pair was implemented using standard MOBILE classes and slight adaptations thereof. For the relative kinematics between the two rigid bodies, a six-degree-of-freedom joint comprising the concatenation of three translational joints and three rotational joints was employed.

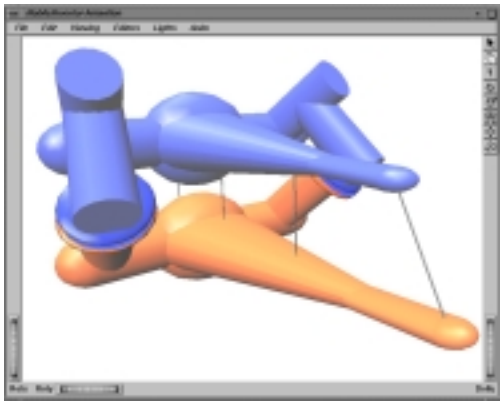

Figure 9: MOBILE model with simplified graphics.

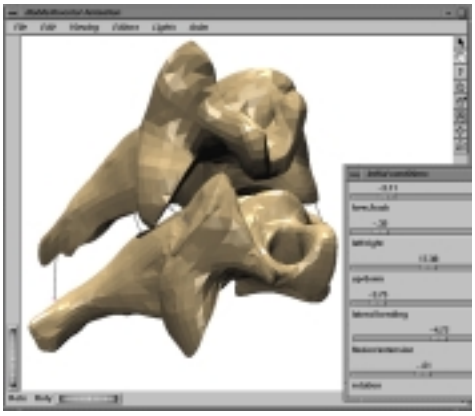

Figure 10: MOBILE model with complex graphics and sliders.

In this setting, two graphical models of different complexity were regarded. One simplified model comprises only cones, cylinders and spheres, giving a rough idea of the vertebrae locations (Fig. 9), The other, more complex model, employs original 3D vertebra visual geometry from Viewpoint® Digital™ and hence renders a more realistic view of vertebrae motion, which can be used for example for understanding the effects of implants or for training purposes (Fig. 10). Both models build upon the *OpenInventor* features of an SGI workstation and are completely independent of the contact iterations. Hence, the user can switch easily

between them by making an appropriate selection in the operation interface. In contrast to the MADYMO model, the MOBILE software package allows online user interactions during the animation. This is achieved through software slider controls, by which system parameters can be changed interactively. For example, the mechanism response can be controlled visually while stiffness properties of the intervertebral disc are changed. Moreover, it is possible to write the program in such a way that all parameters are read from data files, hence allowing for easy variation of data without having to re-compile the program. In addition to this, it is possible to make parameter variations within the program itself. For the effects of the intervertebral disc, the MOBILE-supplied spring-damper element was adapted, allowing for different stiffnesses depending on the sign of the relative displacement in order to implement hysteresis behavior. Similarly, the force-displacement laws for the ligaments were implemented using a derivation of the MOBILE standard class `MoTableSpringDamper` which allows for the required nonlinear viscoelastic behavior.

4.2 Impact Analysis

In order to obtain efficient and accurate computer models, a set of impact geometry situations was investigated. In this setting, the element `MoRegImpCircleCircle`, proved to be extremely useful for the present problem. The basic idea is to regard the facet joints as the end faces of two cylinders touching each other. This assumption seems justified due to the almost flat shape of the articulated surfaces, and proved to be sufficiently accurate in the ensuing simulations. The contact interaction at the facet joints can hence be regarded as a cylinder-cylinder pair, which again renders three possible contact situations: (1) the edge of the upper cylinder touches the flat end of the lower cylinder (Fig. 11); (2) the edge of the upper cylinder touches the egde of the lower cylinder (Fig. 12); (3) the edge of the lower cylinder touches the flat end of the upper cylinder (not shown); and (4) both flat ends of the cylinders rest flatly upon each other.

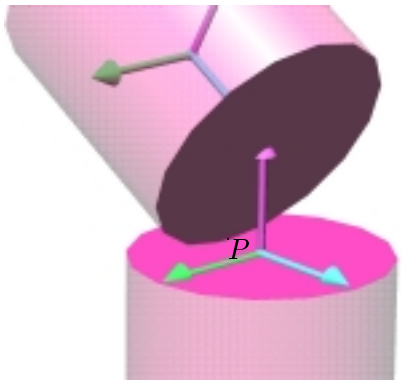

Figure 11: Edge-face contact.

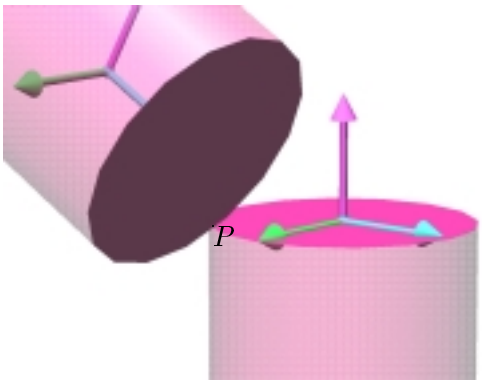

Figure 12: Edge-edge contact.

For edge-edge contact, referring to Fig. 13, the following relationships hold.

Let r_1 and r_2 be the radii of the circles. Moreover, let a_1 and a_2 be the distances of the two circle midpoints to the common line of intersection of the disc planes. One obtains

$$a_1 = \frac{(\mathbf{c}_2 - \mathbf{c}_1) \cdot \mathbf{n}_2}{\mathbf{u}_{a1} \cdot \mathbf{n}_2} = \frac{\mathbf{c} \cdot \mathbf{n}_2}{\mathbf{u}_{a1} \cdot \mathbf{n}_2} \,, \tag{5}$$

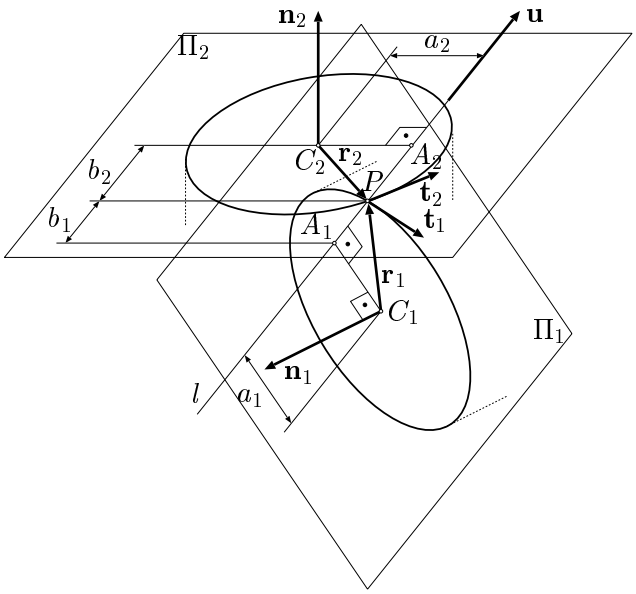

Figure 13: Frictionless circle-circle contact.

and

$$a_2 = \frac{(\mathbf{c}_1 - \mathbf{c}_2) \cdot \mathbf{n}_1}{\mathbf{u}_{a2} \cdot \mathbf{n}_1} = -\frac{\mathbf{c} \cdot \mathbf{n}_1}{\mathbf{u}_{a2} \cdot \mathbf{n}_1} \ , \tag{6}$$

where $\mathbf{c} = \mathbf{c}_2 - \mathbf{c}_1$ is the vector from C_1 to C_2, $\mathbf{n}_1$ and $\mathbf{n}_2$ are the plane normals of circle 1 and 2, respectively, and $\mathbf{u}_{a1}$ and $\mathbf{u}_{a2}$ are unit vectors in direction of the perpendicular distance from the circle midpoints C_1 and C_2 to the common line of intersection of the disc planes, respectively.

Using the quantities described above, the distances b_1 and b_2 from the feet of the circle midpoints at the common line of intersection of the disc planes to the contact point P can be readily computed as

$$b_{1,2} = \sqrt{{r_{1,2}}^2 - {a_{1,2}}^2} \ . \tag{7}$$

Note that b_1 and b_2 are real whenever the common line of intersection of the disc planes intersects both circles. The distance d between the circles along the common line of intersection of the disc planes can be computed as

$$d = |\mathbf{c} \cdot \mathbf{u}| - (b_1 + b_2); \quad d < 0 \ : \text{penetration} \tag{8}$$

where $\mathbf{u}$ is the unit vector in direction of the common line of intersection of the disc planes. With this quantity, the contact condition becomes

$$b_1 + b_2 = |\mathbf{c} \cdot \mathbf{u}| \ . \tag{9}$$

In the case of an almost flat contact between the cylinder surfaces, the formulas derived above become singular. In this case, one can establish the contact geometry by projecting the circles on the plane normal to the (almost parallel) cylinder axes.

In the following, first the case of contact between the edge of circle 1 and the flat end surface of cylinder 2 is regarded (Fig. 14). The case of contact between circle 2 and the end surface of

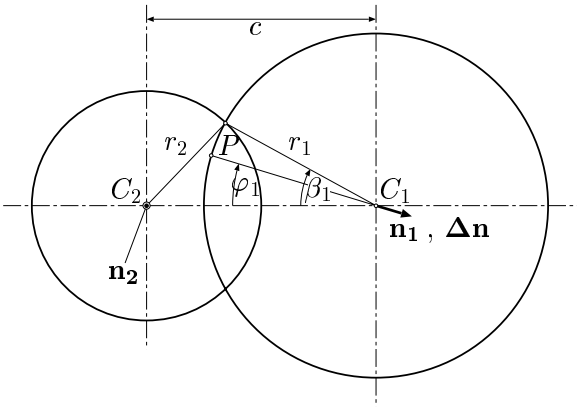

Figure 14: Projection onto contact plane for flat contact.

cylinder 1 is treated analogously. Let P be the contact point and assume that the projection plane is taken as the plane normal to circle 2. The inclination of cylinder 1 with respect to cylinder 2 is assumed to be so small that the distortion of circle 1 to an ellipse is negligible. Contact is maintained whenever the angle φ_1 subtended between the interconnection line of the two circle centers and the ray passing through C_1 and the contact point is less than or equal the angle β_1 subtended between the circle interconnection line and the ray passing through C_1 and the intersection point of both circles.

For the angle β_1, one readily obtains

$$r_2^2 = r_1^2 + c^2 - 2\, r_1\, c\, \cos\beta_1 \qquad \Rightarrow \quad \cos\beta_1 = \frac{1}{2\, r_1\, c}\left(r_1^2 - r_2^2 + c^2\right)\,, \tag{10}$$

where c represents the distance between the centers C_1 and C_2 of the circles. On the other hand, the angle φ_1 can be calculated as

$$\cos\varphi_1 = \frac{-\mathbf{r}_c \cdot \boldsymbol{\Delta}\mathbf{n}}{|\mathbf{r}_c|\,|\boldsymbol{\Delta}\mathbf{n}|}\,, \tag{11}$$

where $\mathbf{r}_c$ stands for the vector from C_1 to C_2 and $\boldsymbol{\Delta}\mathbf{n}$ is the difference of the circle normals, when both are taken as directed into the same half space. However, by taking into account that at contact the surface normals of the two touching cylinders are faced opposite to each other, the above mentioned difference actually becomes the sum of the cylinder normals $\mathbf{n}_1$ and $\mathbf{n}_2$:

$$\boldsymbol{\Delta}\mathbf{n} = \mathbf{n}_1 + \mathbf{n}_2\,. \tag{12}$$

By inserting the above expressions in the contact condition

$$\cos\varphi_1 \geq \cos\beta_1 \tag{13}$$

one obtains

$$\frac{-\mathbf{r}_c \cdot \boldsymbol{\Delta}\mathbf{n}}{|\mathbf{r}_c|\,|\boldsymbol{\Delta}\mathbf{n}|} \geq \frac{1}{2\, r_1\, c}\left(r_1^2 - r_2^2 + c^2\right)\,, \tag{14}$$

or, using $c = |\mathbf{r}_c|$,

$$-\mathbf{r}_c \cdot \boldsymbol{\Delta}\mathbf{n} \geq \frac{1}{2}\,\frac{|\boldsymbol{\Delta}\mathbf{n}|}{r_1}\,\left(r_1^2 - r_2^2 + c^2\right)\,. \tag{15}$$

For a contact of the edge of circle 2 on the end surface of cylinder 1 it holds analogously

$$\mathbf{r}_c \cdot \mathbf{\Delta n} \geq \frac{1}{2} \frac{|\mathbf{\Delta n}|}{r_2} \left(r_2^2 - r_1^2 + c^2\right) . \tag{16}$$

The type of contact is determined by regarding the expressions appearing in the determination of the cosine of angle β_1 and the corresponding angle β_2 for the case of contact of the edge of circle 2 on the end surface of cylinder 1. It holds

$$\frac{1}{2\,r_1\,c}(r_1^2 - r_2^2 + c^2) = \begin{cases} > 1 & : \text{ outside of circle 2} \\ < -1 & : \text{ contact inside of disc 2} \\ \text{else} & : \text{ contact on circle 2} \end{cases} \tag{17}$$

$$\frac{1}{2\,r_2\,c}(r_2^2 - r_1^2 + c^2) = \begin{cases} > 1 & : \text{ outside of circle 1} \\ < -1 & : \text{ contact inside of disc 1} \\ \text{else} & : \text{ contact on circle 1} \end{cases} \tag{18}$$

The above derived formulas fail to be applicable when the circles are fully parallel because in this case the vector $\mathbf{\Delta n}$ vanishes. For this case, one can assume the contact to take place exactly at the center point M of the segment of the center interconnection line contained in the common contact patch, where the distance between C_1 and M is given by

$$L = c - r_2 + \frac{r_1 + r_2 - c}{2} = \frac{c + r_1 - r_2}{2} \quad . \tag{19}$$

For smooth transition between the fully parallel case and the almost parallel case, a novel procedure is proposed, where a virtual contact point is obtained by interconnecting M and P and employing a blending function to position the virtual contact point between these two extremes as a function of the angle between the circle normals. The blending function chosen in the present context is

$$r = r_0\,(1 - e^{-C\,\sin\alpha}), \tag{20}$$

with r_0 being the distance between M and P, C a constant and α the subtended angle between the circle normals.

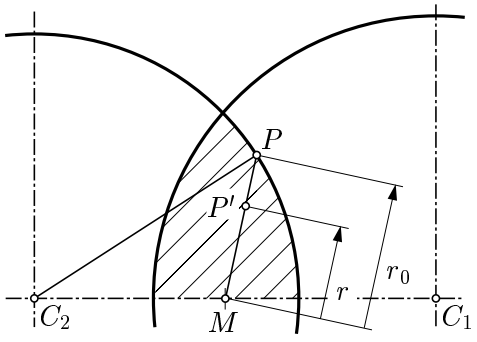

Figure 15: Blending ray within contact patch for flat cylinder-cylinder contact.

The basic idea of the blending function is illustrated in Fig. 16 for the case of a contact of a cylinder with a plane. The virtual contact point P' lies between the center of the cylinder and its circumference along the line of intersection of the common plane of the surface normals $\mathbf{n}_p$

and $\mathbf{n}_c$ and the cylinder end surface through the center of the circle. A particular property of the blending function used is that it renders a stabilizing moment in direction perpendicular to both surface normals that makes fully stable flat contact possible. Hence, no further computations and state transition tracking procedures are necessary for transition from steep to flat contact as well as for transition from one edge to the other. A result of a simulation of the contact between a disc and a plane is displayed in Fig. 17, where the relative indentation r/r_0 (with r_0 being the original disc radius and r the actual distance to the circle center) and the sine of the inclination angle α are plotted over time. Clearly, the motion asymptotically approaches fully flat contact with the virtual contact point at the circle center.

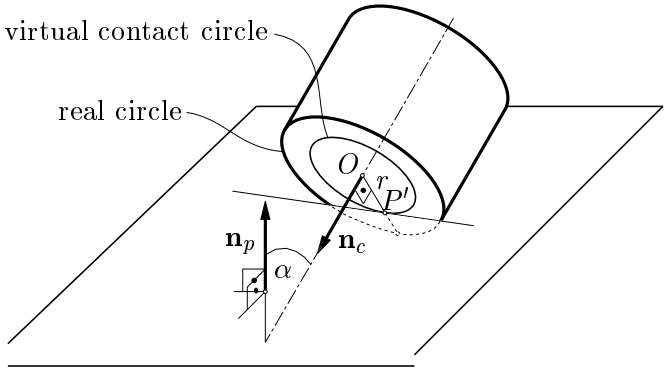

Figure 16: Disc-plane contact.

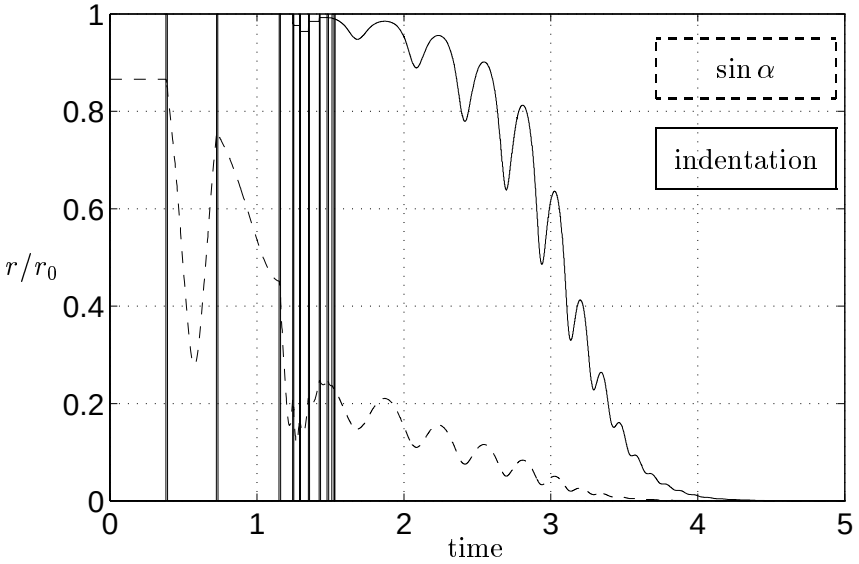

Figure 17: Example of smooth steep-to-flat transition.

Forces As frictionless contact is assumed, the contact force must be aligned with the common line of intersection of the disc planes. In order to take account also of penetration situations, a positive penetration distance d is assumed. The vector $\mathbf{r}_1$ from C_1 to the contact point P is

then assumed as

$$\mathbf{r}_1 = a_1 \cdot \mathbf{u}_{a1} + (b_1 + \frac{d}{2}) \cdot \mathbf{u}\,, \tag{21}$$

where the term $d/2$ makes P lie in the middle between the two intersection points of the circles with the corresponding end face planes. Note that for this to hold true the vector $\mathbf{u}$ must be chosen such that $\mathbf{c} \cdot \mathbf{u} > 0$. This can always be assured by choosing an appropriate sign in the formula for calculation for $\mathbf{u}$, i.e., in

$$\mathbf{u} = \pm \frac{\mathbf{n}_1 \times \mathbf{n}_2}{\| \mathbf{n}_1 \times \mathbf{n}_2 \|} \quad . \tag{22}$$

The position of P with respect to C_2 is obtained accordingly by the vector

$$\mathbf{r}_2 = (\mathbf{c}_1 + \mathbf{r}_1) - \mathbf{c}_2 = \mathbf{c}_1 - \mathbf{c}_2 + \mathbf{r}_1 = \mathbf{r}_1 - \mathbf{c}\,. \tag{23}$$

5 Model Validation

Both vertebrae pair models developed with the MADYMO package and the MBS MBILE library were compared and validated with the experimental results reported by Moroney [17] and the computer simulation performed by de Jager [5]. The simulations compute the translational and rotational deflections from the reference position of vertebra C5 to the new state of equilibrium for nine loading conditions corresponding to application of a single force (20 N) or moment (1.8 Nm) in direction of each elementary motion of C5. In this setting, the numerical values shown in Table 7 and Fig. 18 were obtained. As it can be seen, a good agreement between the experimental data and the computer models could be achieved. In particular, the simplified MBS MBILE model renders results that are not more inaccurate than the complex MADYMO model. At the same time the MBS MBILE model turns out to be faster then the MADYMO model by a factor of 350.

The reason for this performance enhancement is that, besides using simpler and more efficient mathematical models of the contact mechanics, the calculation of the static equilibrium could be achieved in MBS MBILE in a few iterations using the built-in object `MoStaticEquilibriumFinder`, which works with a Newton-Raphson algorithm. In contrast to this, the MADYMO model required the computation of dynamics for the movable vertebra C5 to approach equilibrium.

Acknowledgments

The support of the present work by the European Community as a Marie Curie Research Training Grant ERBFMBICT983385 is gratefully acknowledged.

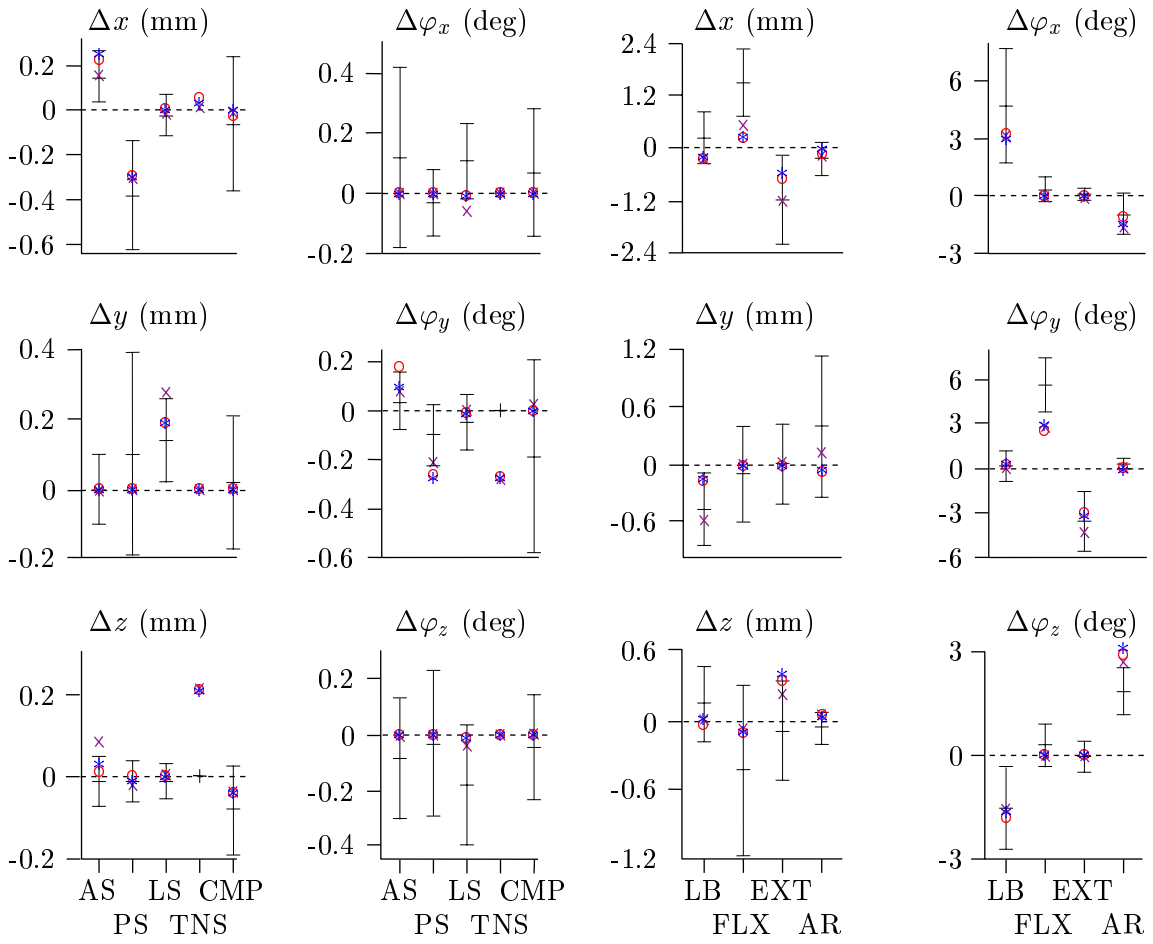

Figure 18: Model comparison of main and coupled displacements: M□BILE: ∘, MADYMO: ∗, de Jager [5]: × with experimental results of Moroney [17]: + (average± SD).

load	model	Δx (mm)	Δy (mm)	Δz (mm)	$\Delta\varphi_x$ (deg)	$\Delta\varphi_y$ (deg)	$\Delta\varphi_z$ (deg)
AS	MOBILE	0.22	0.0	0.01	0.0	0.18	0.0
	MADYMO	0.25	0.0	0.03	0.0	0.10	0.0
	de Jager	0.16	0.0	0.08	0.0	0.07	0.0
	Moroney	0.15	0.0	-0.01	0.13	0.04	-0.08
PS	MOBILE	-0.3	0.0	0.0	0.0	-0.26	0.0
	MADYMO	-0.3	0.0	-0.01	0.0	-0.27	0.0
	de Jager	-0.29	0.0	-0.02	0.0	-0.19	0.0
	Moroney	-0.38	0.11	-0.01	-0.03	-0.09	-0.03
LS	MOBILE	0.0	0.27	0.0	-0.01	-0.01	-0.01
	MADYMO	0.0	0.27	0.0	-0.01	-0.01	-0.01
	de Jager	-0.017	0.27	0.01	-0.06	0.0	-0.04
	Moroney	-0.025	0.14	-0.01	0.11	-0.04	-0.18
TNS	MOBILE	0.05	0.0	0.21	0.0	-0.27	0.0
	MADYMO	0.03	0.0	0.21	0.0	-0.27	0.0
	de Jager	0.0	0.0	0.21	0.0	-0.28	0.0
	Moroney	–	–	–	–	–	–
CMP	MOBILE	-0.03	0.0	-0.04	0.0	0.0	0.0
	MADYMO	0.0	0.0	-0.04	0.0	0.0	0.0
	de Jager	-0.01	0	-0.04	0.0	0.03	0
	Moroney	-0.05	0.03	-0.08	0.06	-0.19	-0.04
LB	MOBILE	-0.29	-0.16	0.03	3.22	0.19	-1.8
	MADYMO	-0.23	-0.14	0.03	2.97	0.3	-1.63
	de Jager	-0.26	-0.59	0.03	3.43	0.0	-1.64
	Moroney	0.25	-0.49	0.16	4.72	0.18	-1.64
FLX	MOBILE	0.21	0.0	-0.1	0.0	2.5	0.0
	MADYMO	0.22	0.0	-0.1	0.0	2.9	0.0
	de Jager	0.43	0.0	-0.08	0.0	2.53	0.0
	Moroney	1.5	-0.1	-0.41	0.25	5.68	0.29
EXT	MOBILE	-0.75	0.0	0.35	0.0	-3.0	0.0
	MADYMO	-0.61	0.0	0.41	0.0	-3.2	0.0
	de Jager	-1.18	0.0	0.2	0.0	-4.42	0.0
	Moroney	-1.18	0.0	-0.08	0.0	-3.66	0.0
AR	MOBILE	-0.18	-0.07	0.06	-1.1	0.02	2.87
	MADYMO	-0.06	-0.04	0.04	-1.43	-0.1	3.1
	de Jager	-0.22	0.1	0.08	-1.49	0.0	2.72
	Moroney	-0.22	0.4	-0.07	-1.0	0.3	1.9

Table 7: Numerical values for Fig. 18.

References

1. Bedewi, P. G. and Bedewi, N. E.: Modeling of occupant biomechanics with emphasis on the analysis of lower extremity injuries. *International Journal of Crashworthiness*, 1(1), Jan. 1996.

2. Bilston, L. E. and Thibault, L. E.: The mechanical properties of the human cervical spinal cord in vitro. *Annals of Biomedical Engineering*, 24:67–74, 1996.

3. Bothema, R. and Roth, B.: *Theoretical Kinematics*. Dover, 1990.

4. Chazal, J., Tanguy, A., Bourges, M., Gaurel, G., Escande, G., Guillot, M., and Vanneuville, G.: Biomechanical properties of spinal ligaments and a histological study of the supraspinal ligament in traction. *Jounal of Biomechanics*, pp. 167–176, 1985.

5. de Jager, M.: *Mathematical Head-Neck Models for Acceleration Impacts*. PhD thesis, Technische Universiteit Eindhoven, 1996.

6. Deng, Y. C.: *Human Head/Neck/Upper-Torso Model Response to Dynamic Loading*. PhD thesis, University of California, 1985.

7. DiAngelo, D., Jansen, T., Eckstein, E., Dull, S., and Foley, K.: Biomechanical analysis of the C1-C2 transarticular screw fixation technique. *Advances in Bioengineering*, BED-Vol. 33, 1996.

8. Foreman, S. and Croft, A.: *Whiplash Injuries, The Cervical Acceleration/Deceleration Syndrome*. Williams & Wilkins, second ed., 1995.

9. Geigl, B. C., Steffan, H., Dippel, C., Muser, M. H., Walz, F., and Svensson, M. Y.: Comparison of head-neck kinematics during rear end impact between Standard Hybrid III, RID Neck, volunteers and PMTOs. In: *Proceedings of the 1995 International IRCOBI Conference on the Biomechanics of Impacts*, pp. 261–270, Brunnen, Switzerland, 1995.

10. Goldsmith, W. and Deng, Y. C.: Numerical evaluation of the three-dimensional response of a human head-neck model to dynamic loading. *SAE Special Publication, Society of Automotive Engineers*, pp. 79–95, 1984.

11. Huston, J. C. and Advani, S. H.: Three-dimensional model of the human head and neck for automobile crashes. *Mathematical Modeling Biodynamic Response to Impact, Society of Automotive Engineers SAE Special Publications*, pp. 9–20, 1976.

12. Jansen, T. H. and DiAngelo, D.: Influences of the location of vertebral IAR on cervical spine kinematics. In: *Proceedings of 16th Southern Biomedical Engineering Conference, Biloxi, MS*. Dept. of Biomedical Engineering, University of Tennessee, Apr. 1997.

13. Kamibayashi, L. K. and Richmond, F. J. R.: Morphometry of human neck muscles. *Spine*, 23(12):1314–1323, 1998.

14. Kecskeméthy, A.: M□BILE 1.3 *User's Guide*. Institut für Mechanik und Getriebelehre, Technische Universität Graz, 1999.

15. Lupker, H. A., de Coo, P. J. A., Nieboer, J. J., and Wismans, J.: Advances in MADYMO crash simulations. Techn. Rep. No. 910879, SAE, 1991.

16. Margulies, S. S., Meaney, D. F., Bilston, L. B., Riederer, S. R., and Campeau, N. C.: In vivo motion of the human cervical spine cord in extension and flexion. In: *Proceedings of the 1992 IRCOBI Conference*, pp. 213–224, Verona, Italy, Sept. 1992.

17. Moroney, S. P., Schultz, A. B., Miller, J. A. A., and Anderson, G. B. J.: Load-displacement properties of lower cervical spine motion segments. *Journal of Biomechanics*, 21:769–779, 1988.

18. Myklebust, J. B., Pintar, F., Yoganandan, N., Cusick, J. F., Maiman, D., Myers, T. J., and Sances, A.: Tensile strength of spinal ligaments. *Spine*, 13:526–531, 1988.

19. Nisan, M. and Gilad, I.: The cervical und lumbar vertebrae—an anthropometric model. *Engineering in Medicine*, 13:111–114, 1984.

20. Obergefell, L. A., Gardner, T. R., Kaleps, I., and Fleck, J. T.: *Articulated Total Body Model Enhancements: User's Guide.* Armstrong Aerospace Medical Research Laboratory, Jan. 1988. Report No. AAMRL-TR-88-043.

21. Panjabi, M. M.: Three-dimensional mathematical model of the human spine structure. *Journal of Biomechanics*, 6:671–680, 1973.

22. Panjabi, M. M.: Cervical spine models for biomechanical research. *Spine*, pp. 2684–2700, 1998.

23. Panjabi, M. M., Duranceau, J., Goel, V., Oxland, T., and Takata, K.: Cervical human vertebrae, quantitative three-dimensional anatomy of the middle and lower regions. *Spine*, pp. 861–869, 1991.

24. Panjabi, M. M., Summers, D. J., Pelker, R. R., Videman, G. E., Friedlaender, G. E., and Southwink, W. O.: Three-dimentional load-displacement curves due to forces on the cervical spine. *Journal of Orthopaedic Research*, 4:152–161, 1986.

25. Pintar, F. A., Myklebust, J. B., Sances, A., and Yoganandan, N.: Biomechanical properties of the human intervertebral disk in tension. *Advances in Bioengineering, American Society of Mechanical Engineers*, pp. 38–39, 1986.

26. Rice, D. P. and MacKenzie, E. J.: The cost of injury in the united states. Techn. rep., Centers for Diseases Control, Washington,DC, 1989.

27. Robin, S., Skalli, W., and Lavaste, F.: Influence of geometrical factors on the behavior of lumbar spine segments: A finite element analysis. *European Spine Journal*, 3:84–90, 1994.

28. Shea, M., Edwards, W., White, A., and Hayes, W.: Variations of stiffness and strength along the human cervical spine. *Journal of Biomechanics*, 24(2):95–107, 1991.

29. Vasavada, A. N., Li, S., and Delp, S. L.: Influence of muscle morphometry and moment arms on the moment-generating capacity of human neck muscles. *Spine*, 23(4):412–422, 1998.

30. White, A. and Panjabi, M. M.: *Clinical Biomechanics of the Spine.* J. B. Lippincott, second ed., 1990.

31. Wismans, J., van Oorschot, H., and Wotering, H. J.: Omni-directional human head-neck response. SAE Paper No. 861893, Society of Automotive Engineers, 1986.